# Near-infrared fluorescence image quality test methods for standardized performance evaluation

Udayakumar Kanniyappan[1,2], Bohan Wang[1], Charles Yang[1], Pejhman Ghassemi[2], Quanzeng Wang[2], Yu Chen[1], Joshua Pfefer[2]
[1] Fischell Department of Bioengineering, University of Maryland, College Park, MD 20742 USA
[2] Center for Devices and Radiological Health, U.S. Food and Drug Administration, Silver Spring, MD 20993 USA

## ABSTRACT

Near-infrared fluorescence (NIRF) imaging has gained much attention as a clinical method for enhancing visualization of cancers, perfusion and biological structures in surgical applications where a fluorescent dye is monitored by an imaging system. In order to address the emerging need for standardization of this innovative technology, it is necessary to develop and validate test methods suitable for objective, quantitative assessment of device performance. Towards this goal, we develop target-based test methods and investigate best practices for key NIRF imaging system performance characteristics including spatial resolution, depth of field and sensitivity. Characterization of fluorescence properties was performed by generating excitation-emission matrix properties of indocyanine green and quantum dots in biological solutions and matrix materials. A turbid, fluorophore-doped target was used, along with a resolution target for assessing image sharpness. Multi-well plates filled with either liquid or solid targets were generated to explore best practices for evaluating detection sensitivity. Overall, our results demonstrate the utility of objective, quantitative, target-based testing approaches as well as the need to consider a wide range of factors in establishing standardized approaches for NIRF imaging system performance.

**Keywords:**, Epoxy resin phantom, Polyurethane phantom, Quantum dot, Indocyanine Green, Image quality characteristics.

## 1. INTRODUCTION

In the past decade, there have been major advances in fluorescence based imaging techniques for medical diagnostics, including exogenous near-infrared (NIR) fluorophores which enhance the information collected by these devices. NIR excitation and emission wavelengths (690 -1000 nm) represent a region where endogenous tissue fluorescence tends to be low and light penetration is relatively high, due to lower absorption of water, melanin, oxy and de-oxy hemoglobin[1-2]. En-face, or surface NIR fluorescence imaging with digital cameras has been implemented for a wide range of applications, such as metastatic imaging[3], lymph node identification[4,5,6], intraoperative tumor delineation and vascular mapping[7]. While the development of NIR imaging exhibits tremendous potential for clinical improvements, there remains a lack of standardized test methods for objective, quantitative characterization of device performance.

Well-validated tissue-simulating phantoms can facilitate a wide variety of performance evaluation tasks throughout the device life cycle, including early system development, device optimization and inter-comparisons, clinical trial standardization, regulatory clearance, manufacturing quality control, re-calibration, clinical constancy testing, and clinician training, among others. Currently, there are numerous international consensus documents that describe standardized phantom-based test methods for established medical imaging modalities such as MRI, CT and PET[8-10], however, no equivalent documents exist for optical imaging modalities such as NIR fluorescence. Thus, there is a need to identify an optimal set of performance tests that are objective, quantitative, and scientifically rigorous, yet minimally burdensome for users. In this context, we have developed phantom-based test methods to characterize various image quality characteristics of an NIRF imaging system using indocyanine green (ICG) and Quantum dots (Qdots).

Design and Quality for Biomedical Technologies X, edited by Ramesh Raghavachari, Rongguang Liang, Proc. of SPIE Vol. 10056, 100560J · © 2017 SPIE · CCC code: 1605-7422/17/$18 · doi: 10.1117/12.2255867

## 2. METHODS

### 2.1 Near-infrared fluorescence imaging system

The present study investigates the various performance characteristics of custom built NIR fluorescence imaging system which uses an external source (Fig. 2). The source is light-emitting diode (M780L3, Thorlabs, Inc., Newton, NJ) with a 780 nm center wavelength, 30 nm bandwidth. The irradiance at the sample surface was 2 mW/cm$^2$. An 800 nm short-pass filter (84-729, Edmund Optics, Barrington, NJ) was used to reduce the potential of detecting light from the diode. A convex lens and diffuser were used to achieve uniform illumination. A long-pass emission filter with a cut-off wavelength of 825 nm (86-078, Edmund Optics, Barrington, NJ) was secured to the camera. A rack and pinion setup was used to move the camera vertically to perform depth of field measurements

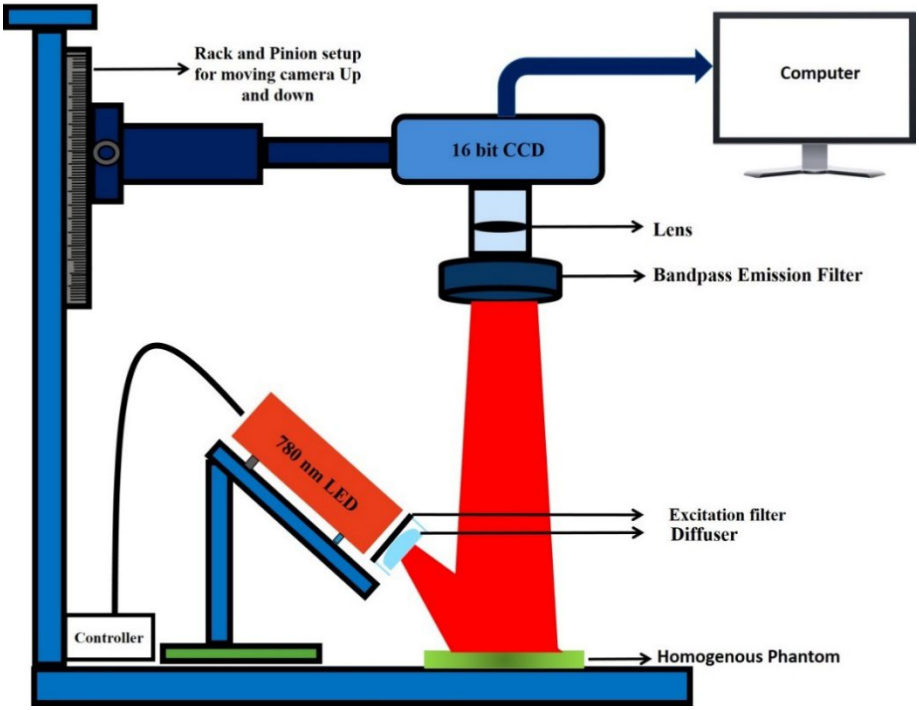


Figure 1. The experimental setup of near infrared imaging system

### 2.2 Wide-Field Phantom

A homogenous fluorescence phantom was necessary to evaluate the uniformity of illumination and the spatial resolution of the system. The matrix materials for the solid uniform phantom were ICG, ethanol, titanium oxide ($TiO_2$) and epoxy resin with hardener. Initially, 15 ml of resin is sonicated with 0.012 g/ml of titanium oxide for 60 minutes. Then, 0.025 mg/ml ICG was added to the mixture and it was further sonicated for 30 minutes. The obtained mixture (resin, titanium oxide and ICG) were then combined with 15 ml of hardener. The final mixture was stirred for 30 minutes to achieve a homogenous distribution of scattering particles. Then, the mixture was poured into 3”x 6”x 1 1/6” molds (Environmental Technology Inc. Fields Landing, CA) and kept in a low-pressure vacuum to remove bubbles. The phantom was allowed to cure for 24 hours before measurements were taken.

### 2.3 Multi-Well phantoms

The Multi-well phantom were widely used to study the sensitivity/linearity and signal-to-noise ratio of the imaging system. The epoxy resin well phantom was prepared by following a 1:1 (resin: hardener) ratio by weight (Easy Cast, Environmental Technology, Inc, Fields Landing, CA). Prior to the experiment, the reduced scattering coefficient of the phantom was calibrated with 10 cm-1 to replicate the tissue scattering environment. The matrix materials used for the epoxy resin phantom were ICG (fluorophore), titanium dioxide ($TiO_2$), resin, and hardener. The ICG concentration was varied from 0.006 µg/ml to 40 µg/ml (13 concentration well phantom). The phantoms were prepared in the following way: the resin with titanium oxide was calibrated with a reduced scattering coefficient of 10 cm$^{-1}$. The resin: hardener

(1:1) mixture was prepared and ICG solution of 20µg/ml was added to each sample, with the stock concentration ranging from 0 to 40 µg/ml. Then, the mixture was stirred for ten minutes and kept at low pressure to remove any air bubbles in the phantom. After that, the mixture was poured into a black 96-well plate (Thermo Fisher Scientific, USA) and allowed to cure for 24 hours.

The polyurethane phantom was prepared using two-part polyurethane system in a ratio of 100/88 by volume (WC-781 A/B, BJB Enterprises Incorporated, Tustin, CA). Prior to the phantom measurements, the reduced scattering coefficient was fixed at 10 $cm^{-1}$ to replicate the tissue environment. The QD800 (Qdot® 800 ITK™ organic quantum dots (Q21771MP), Grand Island, NY 14072) phantoms were prepared with stock concentrations of 1 nM, 2 nM, 4 nM, 10 nM, 20 nM, and 30 nM. Initially, the polyurethane Part B with 0.598 mg/ml of titanium oxide was mixed with the quantum dot phantom and stirred well. Then, each stock mixture was comprised of 1.88 ml of the phantom mixture (1 ml polyurethane Part A: 0.88 ml polyurethane Part B) was added. Then, the mixture was stirred for 30 minutes and kept at low pressure to remove bubbles from the phantom. Finally, the mixture was poured into the black well plate and allowed to cure for 48 hours.

### 2.4 Image sharpness testing

A modified version of the standard bar chart approach for evaluating image spatial resolution was used. Specifically, a negative, chrome on glass USAF 1951 target (Thorlabs Inc., NJ) was placed on top of the wide-field ICG phantom. The 785 nm LED light source was then used to illuminate the target. The contrast transfer function (CTF) was calculated using the formula:

$$\boldsymbol{C_I = \frac{(I_{max} - I_{min})}{(I_{max} + I_{min})}} \quad \textbf{[1]}$$

The CTF was then measured over a wide range of spatial frequencies, and the Rayleigh criterion was used to determine the spatial resolution in horizontal and vertical directions. Measurements were performed at the best focus distance at the center and then, the camera is moved vertically for depth of field measurements [11].

### 2.5 Sensitivity testing

In most cases, sensitivity of the imaging system is evaluated using multi-well phantom approach using NIR emitting fluorophores[1,2]. The mean fluorescence intensity is calculated over a circular area of 50x50 pixels in which the circle is centered where the maximum intensity lies. Prior to that, each image is processed with flat-field correction to avoid uneven illumination of the sample using the following relation:

$$\boldsymbol{I_3 = \left[\frac{I_1}{I_2}\right] x (k_1 + k_2)} \quad [2]$$

Where, $I_1$ = Experimental image; $I_2$ = Reference Image; $K_1$ =Mean fluorescence Intensity; $K_2$ = 0

The signal to noise ratio (SNR) is calculated by measuring the phantom with no concentration as a background ($S_B$), mean fluorescence intensity ($S_I$) and standard deviation of the background well ($S_D$). The signal to noise ratio is calculated using the following relation (3):

$$\mathbf{SNR} = \frac{\mathbf{S_I - S_B}}{\mathbf{S_D}} \quad [3]$$

## 3. RESULTS AND DISCUSSSION

### 3.1 Phantom Characterization

The Fig. 2 show excitation and emission spectral profiles for ICG in presence of solid (cured with epoxy resin) phantom and liquid (Ethanol) phantom. ICG in ethanol shows four peaks (680 nm, 715 nm, 730 nm and 770 nm) whereas in solid ICG (epoxy resin phantom) excitation spectra indicate weaker emission in the 700-775 nm range and fewer peaks. Fluorescence emission spectra (Fig. 2b) show characteristic ICG peaks[12], however, the liquid form exhibits a peak at 820 nm while the solid phantom shows a peak at 800 nm with the spectral shift of ~20 nm. The absolute fluorescence intensity of the liquid phantom exhibits two-fold increase in intensity than that of solid phantom (Fig. 2a). On the other hand, the fluorescence emission spectra of liquid phantom exhibit insignificant variation between liquid and solid

phantom. Similarly, figure 2(c) shows excitation and (d) emission spectrum for quantum dot (QD800) for solid (polyurethane phantom) and liquid form (QD800 in hexane). Broad emission at 800 nm was observed. The absolute variation in the fluorescence excitation intensity of solid phantom exhibit two-fold higher than that of liquid phantom. Similarly, the variations in the absolute intensity of the emission spectra exhibit insignificant/less. Both the excitation and emission peaks were related to characteristics peaks of quantum dots[13]. Furthermore, the quantum dots in hexane exhibit a small red shift in the polyurethane phantom.

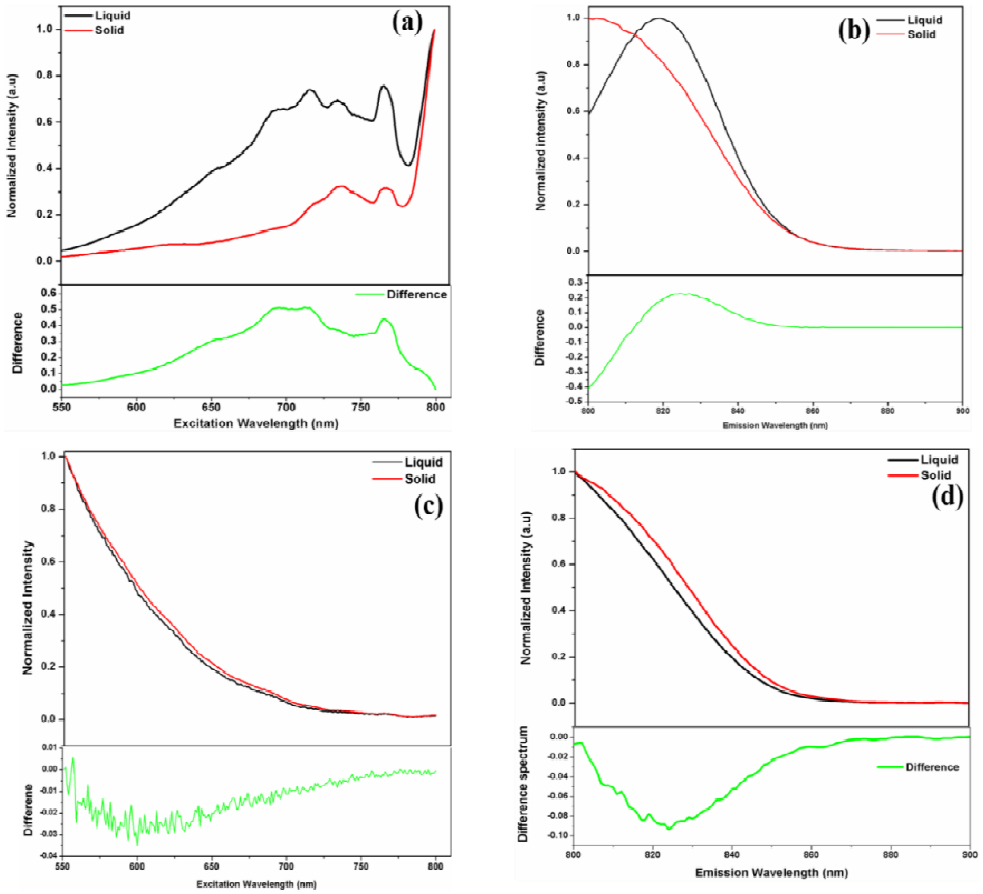


Figure 2. Fluorescence excitation (a, c) and emission (b, d) spectra for ICG (a, b) and quantum dots (c, d) in solid and liquid forms. The ICG excitation spectra were obtained at an 800 nm emission wavelength and the emission spectra were measured at a 785 nm excitation wavelength. The quantum dot (QD800) excitation spectra were measured at an 820 nm emission wavelength and the emission spectra were measured at a 785 nm excitation wavelength. The concentration of ICG is 2.5µg/ml and the concentration of quantum dots is 10 µM.

The excitation and emission matrix (EEM) was also obtained for ICG (Fig. 3a) and quantum dots (Fig.3b). The EEM for ICG was measured in the wavelength region of 700 to 900 nm for excitation and 700 nm – 850 nm for emission with intervals of 5 nm and 1 nm, respectively. Figure 4 (a) shows a broad emission peak around 810 ± 10 nm when it is excited with a ~790 nm wavelength. On the other hand, Figure 4b exhibits a broad emission peak around 800 ± 15 nm when it is excited by a ~770 nm wavelength.

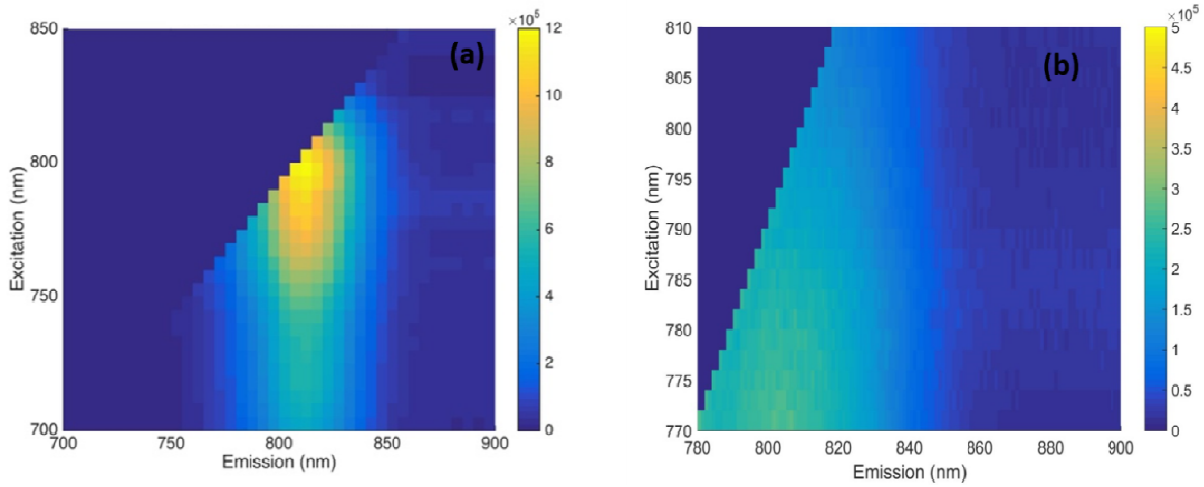


Figure 3. The contour plot shows the excitation and emission matrix (EEM) for (a) Indocyanine Green (b) Quantum dot. The solvent for ICG and Quantum dot is ethanol and hexane, respectively. Excitation scans were performed over 700 -850 nm and emission scans were performed over 700 - 900 nm for ICG. The excitation and emission scan was performed over 770 - 810 nm and 780 - 900 nm emission for quantum dots. The increment for excitation and emission were 5 nm and 1 nm, respectively, with an integration time of 0.5 sec.

Fluorophore photobleaching can cause variations in signal intensity that adversely impact standardized testing. Therefore, fluorophore photo-stability was evaluated to ensure that phantoms produced constant signal levels over time when illuminated with the excitation light source. To assess this parameter, the highest concentration wells from the multi-well plates (ICG is 2.5 µg/ml and of quantum dots is 10 nM) used for sensitivity testing were measured by the camera while under 2 mW/cm$^2$ irradiance. Results in Figure 4 indicate a high degree of stability over a time interval relevant to device testing.

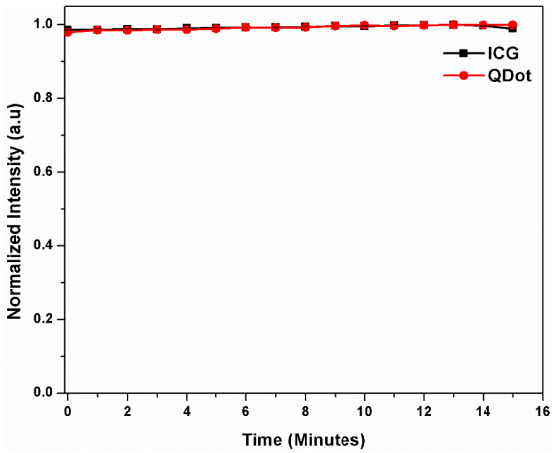


Figure 4. Photobleaching effect over time for quantum dots vs ICG in liquid (a) and (b) solid phantom.

### 3.2 Spatial Resolution

Images of the USAF 1951 resolution target on the turbid ICG-doped phantom were used to evaluate spatial resolution[14]. Preliminary results from our NIRF imaging system are presented in Fig 5. Visual inspection of this image provides qualitative evidence of the high degree of sharpness in NIRF images. The intensity data from this image was used to generate a contrast transfer function, which was in turn used to identify the spatial resolution. The horizontal spatial resolution was found to be 157 µm and vertical resolution was 145 µm[11]. The camera was translated perpendicularly to the resolution target so as to evaluate the depth of field of the system. A set of bars representing a spatial frequency of

2 lp/mm were imaged during this procedure, and are shown in Fig. 5b providing qualitative evidence of changes in resolution through the focal plane.

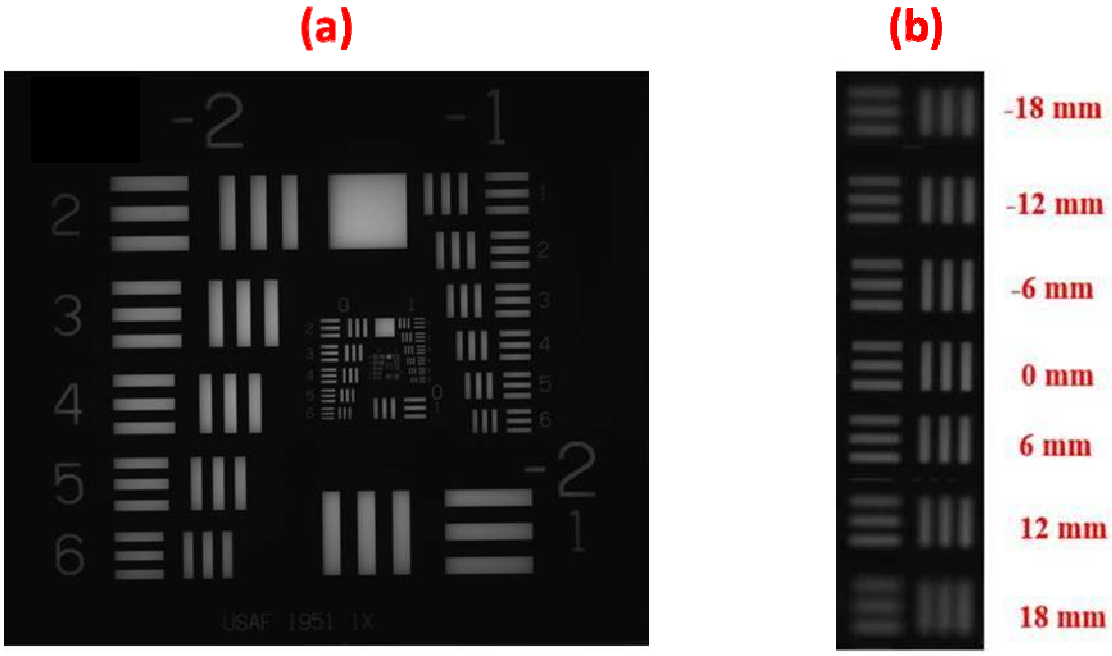


Figure 5. Resolution target images for best focus (a) and single bar pattern (2 lp/mm) as a function of distance from focal plane for evaluation of depth of field

### 3.3 Sensitivity

Phantom measurements were performed to evaluate the sensitivity of the imaging system to detect a minimal concentration of fluorophore. For this purpose, we constructed two different multi-well plate phantoms: (a) Epoxy resin with indocyanine green and (b) Polyurethane with quantum dots. The use of a black well plate has the advantage of reducing unwanted signals that may increase with reflectance off the walls. Further, this study is extended to compare the sensitivity of the system based on two different fluorophores. Figure 6 shows the individually normalized image for each concentration with three different exposure times: 100, 500 and 1000 ms. These images illustrate the degree to which fluorophore concentration and exposure duration affect detectability. For high concentrations, the phantom-filled wells are clearly visible with relatively minimal noise in adjacent regions. As concentration decreases, more variability is seen within the well region and the discrepancy between the ICG-filled regions and the background decreases. Visually, it is difficult to identify the presence of the ICG-filled well at concentrations below 0.4, 0.1 and 0.04 µg/ml, for exposure durations of 100 ms, 500 ms and 1 sec. Previously, Gan et al[12] reported the fluorescence intensity with respect to ICG concentration ranging from 0.1 µg/ml to 100 µg/ml in aqueous solution. The fluorescence intensity at 9 µg/ml reaches its maximum and starts to decrease its intensity due to saturation. Similarly, Liu et al[15] reported the near infrared fluorescence for ICG in DMSO water solution to calibrate the sensitivity of the near infrared fluorescence goggle system. The ICG in DMSO water was measured ranging from 500 pM to 50 µM with the different irradiance power between 5 mW/cm$^2$ and 10 mW/cm$^2$. The threshold concentration for 5 mW/cm$^2$ is 1 µM and for 10 mW/cm$^2$ is 500 nM. For the quantum dot multi-well phantom[16], the fluorescence intensity level of the stock concentration is much lower, thus QD-filled wells are only visually distinguishable in the 500 and 1000 ms images (Figure 7).

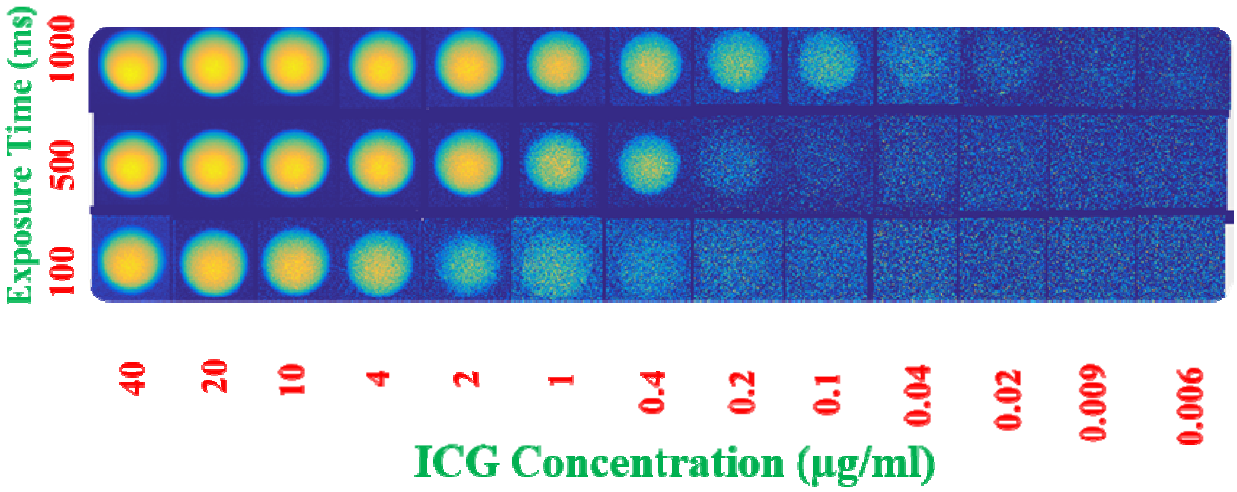


Figure 6. Normalized images of the multi-well ICG-doped epoxy resin phantom of different exposure times (i.e., 100 ms, 500 ms, and 1000 ms).

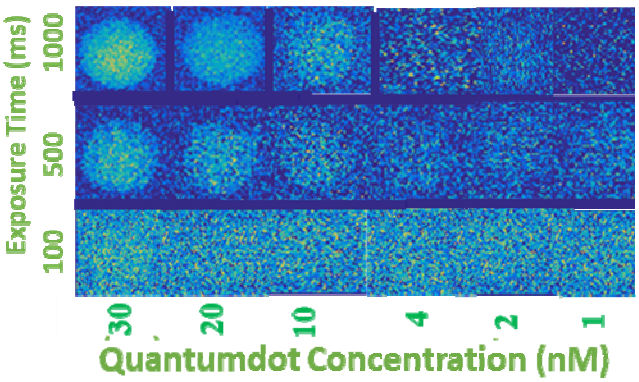


Figure 7. Normalized images of the quantum dot multi-well phantom show various concentrations of quantum dots (1, 2, 4, 10, 20 and 30 nM) with different exposure times.

## 4. CONCLUSION

Our findings indicate that with some additional research, best practices for phantom-based testing of NIRF imaging device performance can be identified for evaluation of key characteristics that impact clinical effectiveness. It is likely that modified versions of the approaches described here may be suitable for incorporation into future consensus standards to encourage rigorous, science-based inter-comparison of NIRF image quality in a range of platforms.

## ACKNOWLEDGMENTS

The authors gratefully acknowledge funding support from the NSF-FDA Scholar-in Residence program (CBET-1445701).

Disclaimer: The mention of commercial products, their sources, or their use in connection with material reported herein is not to be construed as either an actual or implied endorsement of such products by the Department of Health and Human Services.

## REFERENCES


[1] Zhu, B., Sevick-Muraca, E. M., "A review of performance of near-infrared fluorescence imaging devices used in clinical studies," Br J Radiol 88, 20140547 (2015).

[2] Sevick-Muraca, E. M., Sharma, R., Rasmussen, J. C., Marshall, M. V., Wendt, J. A., Pham, H. Q et al., "Imaging of lymph flow in breast cancer patients after microdose administration of a near-infrared fluorophore: feasibility study," Radiology 246(3), 734–41 (2008).

[3] Yuan, J., Yi, X., Yan, F., Wang, F., Qin, W., Wu, G., Chung, L. W. K, "Near-infrared fluorescence imaging of prostate cancer using heptamethine carbocyanine dyes," Mol Med Rep 11(2), 821–828 (2015).

[4] Unno, N., Nishiyama, M., Suzuki, M., Yamamoto, N., Inuzuka, K., Sagara, D., et al. "Quantitative lymph imaging for assessment of lymph function using indocyanine green fluorescence lymphography," Eur J Vasc Endovascular Surg; 36(2) 230–6 (2008).

[5] Eisenberg, D. P., Adusumilli, P. S., Hendershott, K. J., Chung, S., Yu, Z., Chan, M. K., Hezel, M., Wong, R. J., Fong, Y., "Real-time intraoperative detection of breast cancer axillary lymph node metastases using a green fluorescent protein-expressing herpes virus," Ann. Surg, 243(6), 824–832 (2006).

[6] Tanaka, E., Choi, H. S., Fujii, H., Bawendi, M. G., Frangioni, J. V., "Image-guided oncologic surgery using invisible light: completed pre-clinical development for sentinel lymph node mapping," Ann. Surg. Oncol 13(12), 1671–1681 (2006).

[7] Meric-Bernstam, F., Rasmussen, J. C., Krishnamurthy, S., Tan, I. C., Zhu, B., Wagner, J. L., Babiera, G. V., Mittendorf, E. A., Sevick-Muraca, E. M., "Toward nodal staging of axillary lymph node basins through intradermal administration of fluorescent imaging agents," Biomed. Exp 5(1), 183-196 (2014).

[8] Ihalainen, T, M., Lönnroth, N. T., Peltonen, J. I., Uusi-Simola, J. K., Timonen, M. H., Kuusela, L. J., Savolainen, S. E., Sipilä, O. E., "MRI quality assurance using the ACR phantom in a multi-unit imaging center," Acta Oncol 50(6), 966-72 (2011).

[9] Weisser, G., Lehmann, K.J., Scheck, R., Coppenrath, E., Georgi, M., " Dose and image quality of electron-beam CT compared with spiral CT," Invest Radiol 34(6), 415-20 (1999).

[10] Bouchet, F., Geworski, L., Knoop, B. O., Ferrer, L., Barriolo-Riedinger, A., Millardet, C., Fourcade, M., Martineau, A., Belly-Poinsignon, A., Djoumessi, F., Tendero, K., Keros, L., Montoya, F., Mesleard, C., Martin, A. L., Lacoeuille, F., Couturier, O., "Calibration test of PET scanners in a multi-centre clinical trial on breast cancer therapy monitoring using 18F-FLT," PLoS One 8(3), e581522013 (2013).

[11] Themelis G, Yoo JS, Soh KS, Schulz R, Ntziachristos V," Real-time intraoperative fluorescence imaging system using light-absorption correction", J Biomed Opt. 2009 Nov-Dec;14(6):064012.

[12] Gan, Q., Wang, D., Ye, J., Zhang, Z., Wang, X., Hu, C., Shao, P., Xu, R. X., "Benchtop and Animal Validation of a Projective Imaging System for Potential Use in Intraoperative Surgical Guidance," PLoS ONE 11(7), e0157794 (2016).

[13] https://www.thermofisher.com/order/catalog/product/Q21571MP

[14] Zhu, B., Rasmussen, J. C., Litorja, M., Sevick-Muraca, E. M., "Determining the Performance of Fluorescence Molecular Imaging Devices Using Traceable Working Standards With SI Units of Radiance. IEEE Trans Med Imaging," 35(3) 802-11 (2016).

[15] Liu, Y., Njuguna, R., Matthews, T., Akers, W. J, Sudlow, G. P, Mondal, S., Tang, R., Gruev, V., Achilefu, S., "Near-infrared fluorescence goggle system with complementary metal-oxide- semiconductor imaging sensor and see-through display," J Biomed Opt. 18(10), 101303 (2013).

[16] Zhu, B., Rasmussen, J. C., Sevick-Muraca, E. M., "A matter of collection and detection for intraoperative and noninvasive near-infrared fluorescence molecular imaging: To see or not to see?," Med Phys 41(2), 022105 (2014).